Environ. Eng. Res. 2023; 28(1): 210455
https://doi.org/10.4491/eer.2021.455

pISSN 1226-1025
eISSN 2005-968X

Research

Optimization and physicochemical studies of alumina supported samarium oxide based catalysts using artificial neural network in methanation reaction

Salmiah Jamal Mat Rosid[1†], Azman Azid[2], Aisyah Fathiah Ahmad[2], Nursyamimi Zulkurnain[2], Susilawati Toemen[3], Wan Azelee Wan Abu Bakar[3], Ahmad Zamani Ab Halim[4], Wan Nur Aini Wan Mokhtar[5], Sarina Mat Rosid[6]

[1]*Unisza Science and Medicine Foundation Centre, Universiti Sultan Zainal Abidin, Gong Badak Campus, 21300 Kuala Nerus, Terengganu, Malaysia*
[2]*Faculty of Bioresources and Food Industry, Universiti Sultan Zainal Abidin, Besut Campus, 22200 Besut, Terengganu, Malaysia*
[3]*Department of Chemistry, Faculty of Science, Universiti Teknologi Malaysia, 81310 UTM Skudai, Johor, Malaysia*
[4]*Faculty of Industrial Sciences & Technology, Universiti Malaysia Pahang, 26300 Gambang, Kuantan, Pahang, Malaysia*
[5]*School of Chemical Sciences & Food Technology, Faculty of Science and Technology, Universiti Kebangsaan Malaysia, 43600 Bangi, Selangor, Malaysia*
[6]*Advanced Membrane Technology Research Centre (AMTEC), Universiti Teknologi Malaysia, 81310 UTM Skudai, Johor, Malaysia*

Received September 17, 2021 **Revised** January 27, 2022 **Accepted** February 08, 2022

ABSTRACT

Developed countries are increasing their demand for natural gas as it is an industrial requirement for fuel transportation. Most of modern society relies heavily on vehicles. However, the presence of CO_2 gas has led to the categorization of sour natural gas which reduces the quality and price of natural gas. Therefore, the catalytic methanation technique was applied to convert carbon dioxide (CO_2) to methane (CH_4) gas and reduce the emissions of CO_2 within the environment. In this study, samarium oxide supported on alumina doped with ruthenium and manganese was synthesized via wet impregnation. X-ray diffraction (XRD) analysis revealed samarium oxide, Sm_2O_3 and manganese oxide, MnO_2 as an active species. The reduction temperature for active species was at a low reaction temperature, 268.2°C with medium basicity site as in Temperature Programme Reduction (TPR) and Temperature Programme Desorption (TPD) analyses. Field Emission Scanning Electron Microscopy (FESEM) analysis showed an agglomeration of particle size. The characterised potential catalyst of Ru/Mn/Sm (5:35:60)/Al_2O_3 (RMS 5:35:60) calcined at 1,000°C revealed 100% conversion of CO_2 with 68.87% CH_4 formation at the reaction temperature of 400°C. These results were verified by artificial neural network (ANN) with validation R^2 of 0.99 indicating all modelling data are acceptable.

Keywords: Artificial neural network, Carbon dioxide, Catalyst, Methanation, Samarium

1. Introduction

Energy demand for natural gas has increased from 2005 until present for household usage, transportation, electrical and industry. This is because natural gas is the cleanest option among fossil fuels and emits less CO_2 into the atmosphere [1]. As part of the Kyoto Protocol, Malaysia's natural gas must be treated in order to minimize the emission of CO_2 gas into the air. The most promising technique to eradicate CO_2 from natural gas is through catalytic methanation, which converts it into CH_4 in the existence of H_2 gas. The basic oxides for instance are oxides of rare earth metals which form a good catalyst for the reductive process in the natural

This is an Open Access article distributed under the terms of the Creative Commons Attribution Non-Commercial License (http://creativecommons.org/licenses/by-nc/3.0/) which permits unrestricted non-commercial use, distribution, and reproduction in any medium, provided the original work is properly cited.

Copyright © 2023 Korean Society of Environmental Engineers

† Corresponding author
E-mail: salmiahjamal@unisza.edu.my
Tel: +60139089125
ORCID: 0000-0002-4482-0305

gas conversion reaction [2]. The use of samarium as a promoter or support within the catalytic reaction has been widely investigated due to these interesting properties, i.e. reducibility and basicity. As investigated by Yamasaki et al. [3], the number of active surface nickel sites has increased as samarium was used as a promoter in the Ni-Zr catalyst, thus enhancing the performance of catalytic activity. However, no studies have been conducted on the possible optimization improvement of CO_2 methanation over supported samarium oxide based as a heterogeneous basic catalyst.

During the experiment, the optimization process will be needed in order to identify the optimum parameter that gives higher CO_2 conversion. Thus, modelling of variables in methanation reaction is needed to save time and cost and also give higher predictions of CO_2 conversion. In recent years, artificial neural network (ANN) based modelling has grabbed many attentions in research area especially in an industry for developing empirical models for time series prediction. ANN is a process of information's element, constituted by layers of neurons and an output as a result [4, 5]. Due to its high proficiency and unique features, the ANN method has given better predictions and its results depend on the number of variables entered [6].

ANN has been widely used in the industrial hydrogen production plants. A back-propagation feed forward ANN with three layers was used in predicting the optimum parameters of feed temperature, reformer pressure, steam to carbon ratio and carbon dioxide to methane ratio in the feed stream. From the results, the artificial neural network can be easily applied to analyze the performance of the entire hydrogen plant to achieve suitable operating conditions, with less time-consuming and high accuracy [7]. Recently, hydrogen production by catalytic dry reforming of methane through the use of artificial neural networks (ANN) has been reported by Alsaffar et al. [8]. They focused on the optimization of gas hourly space velocity (GHSV), the oxygen (O_2) concentration in the feed, the reaction temperature and the CH_4/CO_2 ratio. The predicted hydrogen yield and the CH_4 conversions by the optimized ANN model were in close agreement with the observed values obtained from the experimental runs.

In the area of CO_2 methanation, Ngo and Lim [9] developed the physics-informed neural networks (PINNs) to solve the catalytic CO_2 methanation in isothermal fixed bed (IFB) model. When only predicting the concentration outside the training domain, PINN showed excellent extrapolation performance with an accuracy of 88.1%. These results indicate that PINN can be used for solution and system identification in a fixed bed model with chemical reaction kinetics. Meanwhile, the study by Esfandyari et al. [10] also found ANN to be a powerful and accurate tool for building up empirical models for prediction in Fischer-Tropsch. Four variables such as operating temperature, operating pressure, time and CO/H_2 ratio have been studied to predict the CH_4, CO_2 and CO compositions. Therefore, the uniqueness of current study is application of supported samarium oxide-based catalyst for CO_2 methanation and its process optimization using an ANN to achieve exact optimal parameters and the prediction of experimental performance. Additionally, the physicochemical characteristic of $Ru/Mn/Sm/Al_2O_3$ (RMS) catalyst was also examined using several characterization techniques.

2. Experimental

2.1. Material and Reagents

In this research, all metals salts used for catalyst preparation were of high purity and were purchased from Sigma Aldrich. A samarium (III) nitrate hexahydrate ($Sm(NO_3)_3.6H_2O$) was used as based catalysts while, manganese nitrate tetrahydrate ($MnNO_3.4H_2O$) and ruthenium(III) chloride ($RuCl_3$) were used as dopant and co-dopant. Then, aluminium oxide bead, γ-Al_2O_3 with 3 mm was used as a support material of catalyst.

2.2. Preparation and Catalytic Activity of $Ru/Mn/Sm/Al_2O_3$ (RMS) Catalyst

The RMS catalyst was prepared by the aqueous incipient wetness impregnation method [11, 12]. A 5 g of $Sm(NO_3)_3.6H_2O$ was weighed in a beaker and dissolved with 10 mL of distilled water. The mixed catalyst solution was prepared by adding the appropriate amount of dopant $MnNO_3$ (0.141 g) and co-dopant $RuCl_3$ (0.289 g) into the based solution to get the desired ratio of RMS (5:35:60). The catalyst was then labelled as RMS (5:35:60) to indicate that there is 60 wt% of Sm, 35 wt% of Mn and 5 wt% of Ru. Then, the mixture catalyst was stirred continuously for 30 min before being immersed with 7 g of 3 mm alumina beads for 1 h. The alumina beads were left in the desiccator overnight, and then aged at 80–90°C overnight in an oven before calcination in the furnace occurred at 400°C for 5 h using a 10°C/min ramp rate. The same procedure was repeated for other Sm loadings of 50–85 wt% and calcination temperatures of 700–1,100°C.

Meanwhile, the catalytic activity testing was performed under atmospheric pressure in a fixed micro-reactor and analysed online by use of a Fourier Transform Infrared from ambient temperatures of up to 400°C of reaction temperature at a ramp rate of 5°C/min. Glass tube made of Pyrex glass with a diameter of 10 mm and a length of 520 mm was used as the catalyst holder and placed in an isothermal furnace. The gaseous mixture of CO_2 and H_2 with a ratio of 1:4 was launched into the reactor system. The formation of CH_4 was measured via a Gas Chromatography Flame Ionisation Detector system equipped with an Ultra 1 capillary column (nominal column 25.0 m × 200 μm × 0.11 μm).

2.3. Characterisation

X-ray Diffraction (XRD) analysis was performed using a Crystalloflex D5000 Diffractometer with CuKα radiation (λ = 1.54060A). The sample was placed into the sample holder with diameter of 10-15 mm and approximate depth of 1 mm in a 40 × 33 × 2 mm glass plate. X-ray Photoelectron Spectroscopy (XPS) analysis was performed via Kratos AXIS Ultra DLD using energy of 15.0 kV. The samples were tested at the electron take-off angle which is normal to the surface working at 20 eV. Electron Spin Resonance (ESR) analysis was conducted using the ThermoFlex3500 model and was operated with a center field of 336 mT, a modulation amplitude of 1.00 × 100, a scan time equal to 4 min with 3 number of scans, and a microwave power of 0.998 mW. Meanwhile, H_2-Temperature Programmed Reduction (H_2-TPR) and CO_2-Temperature Programmed Desorption (CO_2-TPD) analyses were accomplished by using

Micromeritics Autochem 2920. The measurement was carried out by ramping the catalyst sample from room temperature to 1,000°C with a total gas flow of 20 mL/min at 10°C/min. For the Field Emission Scanning Electron Microscopy- Energy Dispersive X-Ray (FESEM-EDX) study, a 15 kV Zeiss Supra 35 VP FESEM coupled with EDX analyzer was used to scan the sample under 25 kV. Lastly, surface area analysis was measured by Nitrogen sorption analysis using a Micromeritics ASAP 2010 at -196°C. Prior to the measurement, the calcined catalysts were degassed at 120°C overnight.

2.4. Statistical Analysis

2.4.1. Artificial Neural Network (ANN)

ANN's most common technique, known as feed forward MLP artificial neural network (MLP-FF-ANN), is one of the techniques that relies on memory less and thus the reflection in response to the result is much faster than the feedback type [13]. In this study, MLP-FF-ANN generated by JMP version 10 (SAS, USA) was used for simulation because of its flexibility and ease of use when compared to the Statsoft Statistica Release 7.0 software [14]. This network type consists of a system of multi-level interconnected "neurons" or nodes that are formed in three layers, namely input layers (independent variables), hidden layers (one or more), and output layers (dependent variables) [15, 16]. The input variables were calcination temperature (°C), based ratio (%) and catalyst dosage (g), while the output was CO_2 conversion (%). The parameters were chosen based on our previous study [11, 17], as they could give great influence on the performance and physicochemical properties of the prepared catalyst. The model was trained by using the Levenberg Marquardt Learning Algorithm [14, 18]. The respected R^2 and RMSE were computed using Eq. (1) and (2), respectively:

$$RMSE = \sqrt{\frac{1}{N}\sum_{i=1}^{N}(t_i - td_i)^2} \quad (1)$$

$$R^2 = 1 - \frac{\sum_{i=0}^{n}(t_i - td_i)^2}{\sum_{i=0}^{n}(t_i - td_i)^2} \quad (2)$$

The predicted value is signified by where t_i the measured value of the experimental samples is, td_i signifies the predicted value, and N represents the total of samples. The range calculation for R^2 is in between 0.0–1.0. The lowermost value of R^2 is considered weak, whilst the highest value (near to 1.0) indicates suitability to be chosen as the best predictor [18]. Next, the efficiency model (EM) by Nash and Sutcliffe [19] was used to test the fit between measured and modelled data using the Eq. (3):

$$E = \frac{\sum_{i=1}^{n}(Q_m - Q_{mea_{avg}})^2 - \sum_{i=1}^{n}(Q_m - Q_p)^2}{\sum_{i=1}^{n}(Q_m - Q_{mea\_avg})^2} \quad (3)$$

Where, E refers to coefficient of efficiency, O_m represents the measured value, Q_p indicates the predicted value and Q_{mea_avg} denotes an arithmetic average measured value. If modelled values perfectly match the measured ones, then E is equal to 1.

3. Result and Discussion

3.1. Characterization

3.1.1. XRD analysis

XRD analysis was performed to observe the presence of active oxide phases on the prepared RMS (5:35:60) catalyst in different calcination temperatures of 400, 700, 900, 1,000 and 1,100°C. Calcination temperature would influence both the crystal phase and crystallite size of the catalyst. Some processes including change in structure, arrangement of crystal lattice and active phase formation could also occur during sintering [11, 20]. The XRD diffractograms of RMS (5:35:60) catalysts calcined at different temperatures as shown in Fig. 1.

As shown in Fig. 1, the phases for RMS (5:35:60) catalysts were highly amorphous and most of them were dominated by alumina support, Al_2O_3 at 2θ values of 66.86°, 45.79°, 37.73°, and 39.42°. The amorphous phases may be due to the presence of the lanthanide element, samarium in the catalyst and may have hindered the crystallinity of the catalyst phase. RMS (5:35:60) catalyst heated at 400°C and 700°C shows similar diffractograms with the presence of alumina cubic peaks only. Meanwhile, RMS (5:35:60) catalysts heated at 900 to 1,100°C showed the existence of tetragonal RuO_2 at 2θ values of 28.08°, 35.09°, and 54.53° besides cubic Sm_2O_3 peaks at 27.88°, 32.31°, and 45.36° in addition to the cubic of Al_2O_3. Interestingly, the presence of new small peaks of MnO_2 with tetragonal phase at 2θ values of 36.99°, 56.40°, and 42.82° were observed for the catalyst calcined at 1,000 and 1,100°C. However, the appearance of low MnO_2 intensity peak in the diffractogram was in accordance with research conducted by Xu et al. [21] who also observed a broad peak of MnO_2 which indicated the amorphous nature of the product. Therefore, 900°C of calcination temperature is not sufficient to increase the crystallinity and size of the MnO_2 species thus, it was not observable in the diffractogram. Besides that, a few peaks on the diffractogram that overlapped each other were also observed. These overlapping peaks occurred due to very similar crystallographic characters from the PDF XRD profile.

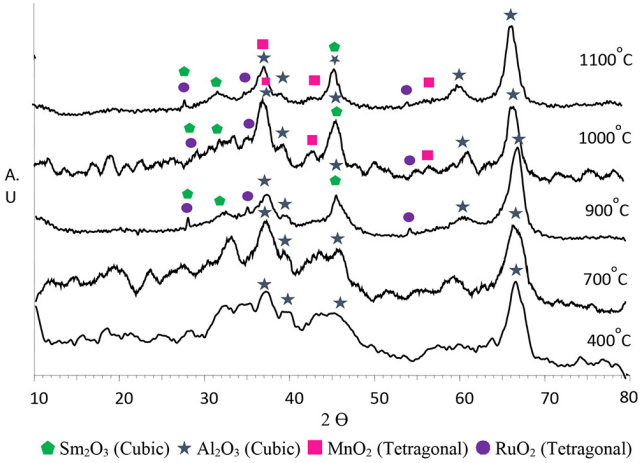

Fig. 1. XRD Diffractograms of RMS (5:35:60) catalyst calcined at (a) 400°C, (b) 700°C, (c) 900°C, (d) 1,000°C and (e) 1,100°C for 5 h.

3.1.2. X-ray Photoelectron Spectroscopy (XPS) analysis

To determine the oxidation state of elements in the catalyst, the relative contents of each state over the catalyst surface were deconvulated using XPS software based on the binding energy. The relative surface charge was adjusted against the C 1*s* line (284.50 eV) as a standard. Fig. 2 shows the deconvulation of XPS spectra for O 1*s*, Al 2*p*, Mn 2*p* and Sm 3*d*. Oxygen constitutes a high percentage in the surface composition, which was 25.42%. The O 1*s* photoemission spectrum exhibited single-lobed envelopes. The deconvulation produced two peaks, which suggests the presence of two different elements. The strongest peak had an E_b value of 531.50 eV and was assigned to Al_2O_3 or oxygen of the Sm^{3+}-O groups. The presence of a weak peak at an E_b value of 529.96 eV was assigned as oxygen of Sm^{2+}-O groups. This is related to the oxygen in the crystal lattice of Sm_2O_3 [22]. Aluminium constituted a high percentage in the surface composition, which was 65.04%, confirming the Al_2O_3 as a support. Deconvulation of Al 2*p* produced two peaks that indicated Al^{3+} in different chemical environments. The E_b values of 73.40 and 74.47 eV, were credited to the presence of Al^{3+} in Al_2O_3 and $Al(OH)_3$, respectively. Meanwhile, Mn 2*p* consisted of two doublets which were Mn $2p_{1/2}$ and $2p_{3/2}$ which are equal to 11.5 eV. In this study, the high binding energy in the range of 642 - 647 eV was ascribed to the presence of Mn^{4+} from the MnO_2 species [23] and was aligned with the observation obtained from the XRD analysis in Fig. 1.

The peak of samarium formed two doublet structures of 3d5/2 and 3d3/2 equal to 28 eV as a result of spin-orbit splitting and their satellites in rare-earth compounds as also explained by Chung et al. [24]. The first doublet corresponded to Sm 3d5/2 at a binding energy of 1,082.33 eV that was attributed to Sm3+ ion under its oxidized form in metal oxide, Sm2O3. The observation of satellite Sm2O3 shouldered at 1,085.73 eV was associated with a strong charge-transfer effect, which leads to an increase in the number of unpaired 4f electrons by more than one of the samarium oxides [25]. It was also reported that Sm was in a trivalent state when adsorbed onto transitional metals due to the close binding energy at 1,082.33 and 1,085.73 eV [26, 27]. This is supported with XRD where Sm_2O_3 was observed in the diffractograms.

3.1.3. Electron Spin Resonance (ESR) analysis

The ESR spectra of the RMS (5:35:60) catalyst calcined at various temperatures are shown in Fig. 3. From the spectra, all of the catalysts showed a g value of 2.12 with different intensities. The shift from the value was caused by the electron spin-orbit interaction in atomic orbital. The 'wing' that forms from both sides at the g value of 2.12 was attributed to Mn^{4+} as suggested by Chakradhar et al. [28]. This result correlates well with the result obtained from the XRD and XPS analysis in Fig. 1 and 2 whereby the manganese species that exists in this catalyst were MnO_2 (Mn^{4+}). This result is similar to Phan et al. [29] who identified that MnO_2 will exhibit a symmetrical center which is caused by a paramagnetic property at a magnetic field about 300 mT. From the ESR spectra, at calcina

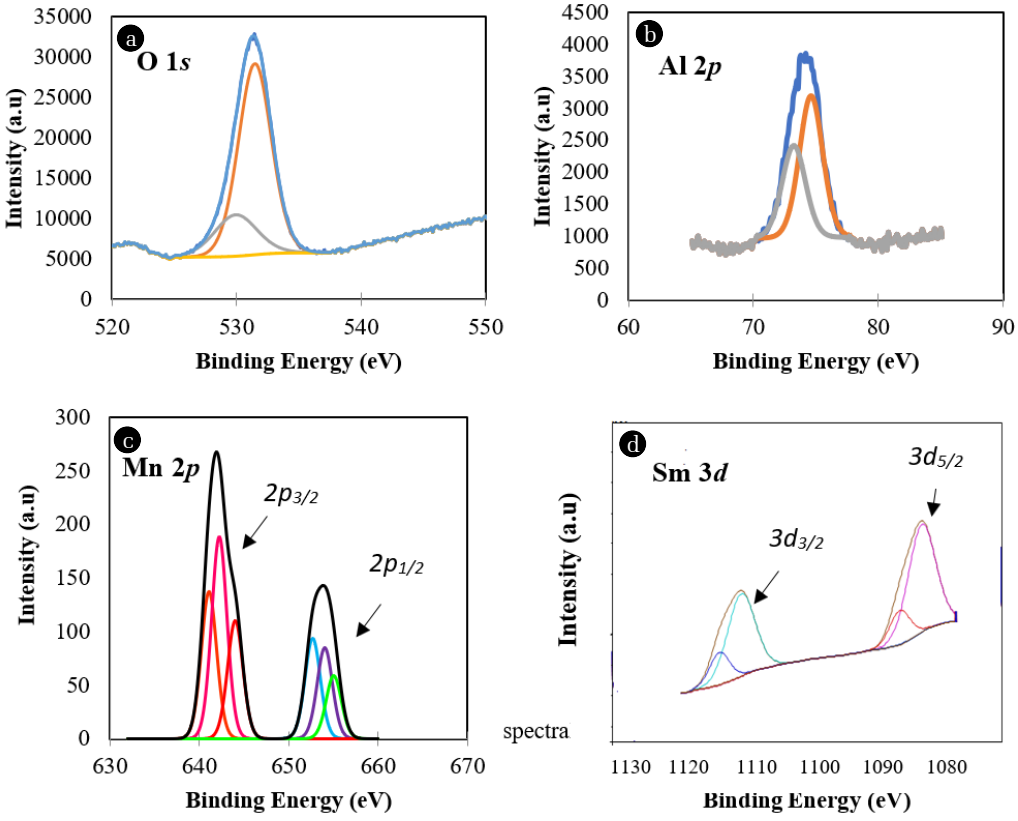

Fig. 2. Binding energy for elements of O 1*s*, Al 2*p*, Mn 2*p*, Sm 3*d* over RMS (5:35:60) catalyst calcined at 1,000°C for 5 h.

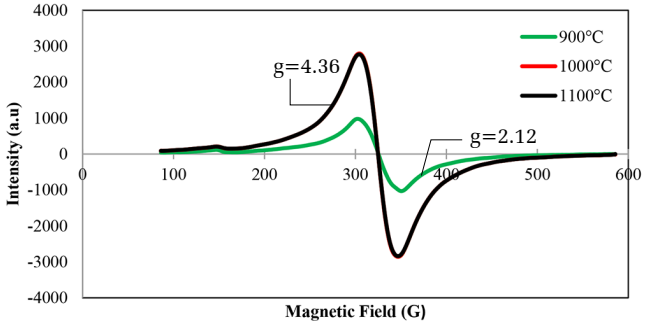

Fig. 3. Overlay of ESR spectra over RMS (5:35:60) catalyst calcined at 900, 1,000, and 1,100°C for 5 h.

tion temperatures of 1,000°C and 1,100°C, both peaks overlapped and exhibited the highest peak intensity as compared to 900°C. It can be clearly seen in XRD diffractograms that the presence of MnO_2 peaks in the catalyst calcined at 1000 and above. However, the peak of MnO_2 was not detected in XRD analysis calcined at 900°C which can be explained by the lower signal ESR peak due to lower intensity and crystallinity of the MnO_2 species. Therefore, the paramagnetic properties of the catalysts were said to be higher at 1,000°C and 1,100°C which could contribute to the maximum catalytic activity of CO_2 conversion.

3.1.4. H_2-Temperature Programmed Reduction (H_2-TPR) analysis

A H_2-TPR analysis was performed to provide information on the reducibility of various chemical species contained in the catalyst, the degree of interaction between metal-support, and to determine the reduction temperature. The H_2-TPR profile of RMS (5:35:60) was depicted in Fig. 4. The H_2 consumption of the profile provides a cursory measure level of coordination and availability of the surface capping oxygen ions in the catalyst [30].

At calcination temperatures of 900, 1,000 and 1,100°C, four reduction peaks were detected at 268.2, 433.5, 594.2, and 976.7°C, respectively. The first reduction peak at 268.2°C was owing to the reduction temperature of RuO_2 reduction to metal Ru where the H_2 consumption was 0.12 cm^3/g STP [31]. It can be observed that only a tiny amount of H_2 was consumed on the catalyst. As

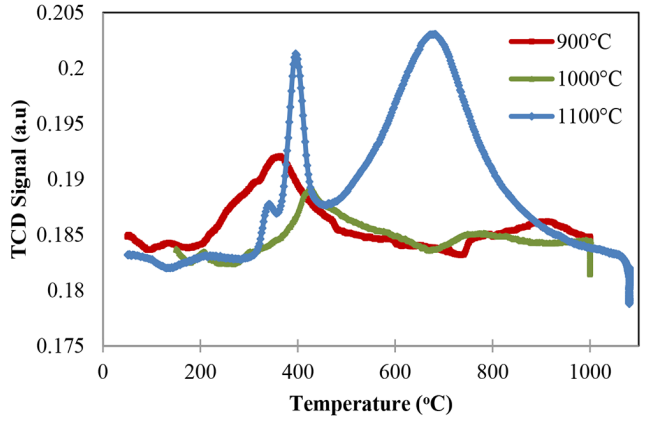

Fig. 4. H_2-TPR profile of RMS (5:35:60) at 900°C, 1,000°C and 1,100°C calcination temperatures.

observed by Peluso et al. [32], the second reduction peak at 433.5°C of H_2 consumption, 0.02 cm^3/g STP belonged to the reduction of Mn^{4+} to Mn^{2+}. On the other hand, the reduction peak at 594.2°C was due to the reduction of the Mn-O-Al species with a total H_2 consumption, of 0.02 cm^3/g STP [33]. The last reduction peak at 976.7°C was consigned as the bulk oxygen reduction from SmO_2 to Sm_2O_3 where the amount of H_2 consumption was recorded as 0.13 cm^3/g STP. The reduction peaks at 1,100°C showed a shift to higher temperatures, implying stronger interactions between active species and alumina support which led to a decrease in reducibility. The outflow of H_2 to the catalyst surface increased the H_2 adsorption area and improved the hydrogenation activity. The H_2-TPR profile demonstrated that γ-Al_2O_3 was also an inert carrier, so no reduction peak of γ-Al_2O_3 was observed [34].

3.1.5. CO_2-Temperature Programmed Desorption (CO_2-TPD) analysis

A CO_2-TPD analysis was done to study the basicity of the catalyst surface and determine the CO_2 and H_2 sorption profiles on its surface. Lin et al. [35] found that supported noble metal catalysts have strong metal-support interactions, which affects the performance of active species, and favors the adsorption through electron-deficient state of metal nanoparticles. The difference in desorption profile was caused by the coordination of CO_2 to metal oxides with different energies. The CO_2-TPD profiles were depicted in Fig. 5.

The peak at the lowest temperature of 117.6°C was due to desorption of low chemisorption or physical adsorption of CO_2 on the catalyst surface [36]. Nevertheless, the peaks at 210.6°C and 279.4°C could be ascribed to the inorganic carboxylate desorbed on the surface of the catalyst as suggested by Cox [37]. In addition, the TPD profile's peak area of CO_2 desorbed from the surface is used to determine the catalyst's total basicity. Therefore, the broad peak areas at 210.6°C and 279.4°C indicated higher basicity surface of catalysts due to many CO_2 gas desorbed on the basic sites of the catalyst. Aside from that, the amount of CO_2 adsorbed on the catalyst at 1,000°C was also the highest at 210.6°C and 279.4°C with 48.62 cm^3/g and 34.00 cm^3/g at STP respectively. As a result,

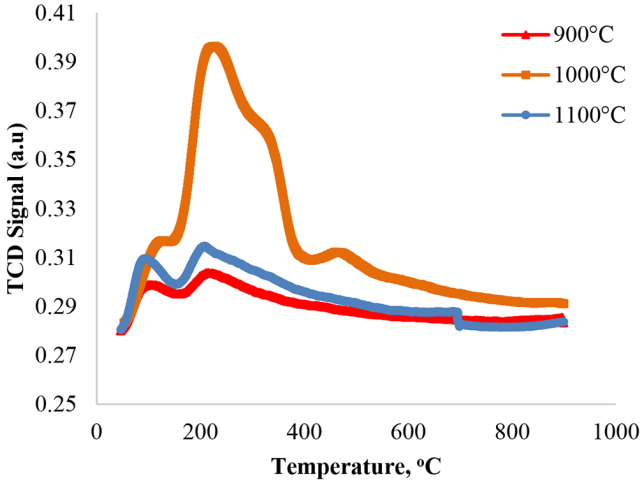

Fig. 5. CO_2-TPD curve of RMS (5:35:60) calcined at 900°C, 1,000°C and 1,100°C for 5 h.

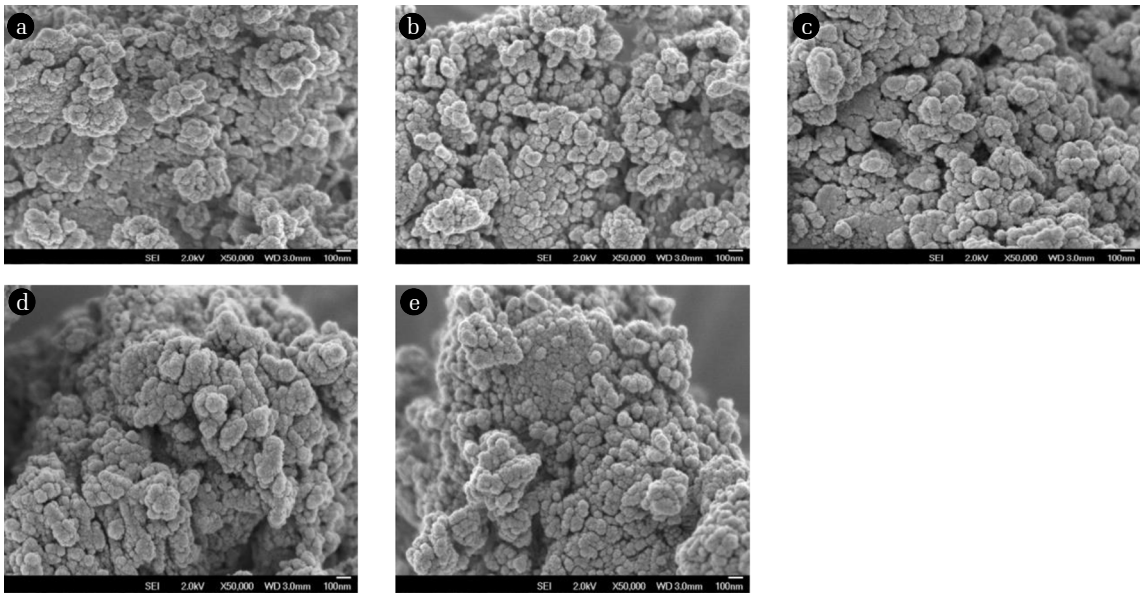

Fig. 6. FESEM micrographs of RMS (5:35:60) catalyst calcined at (a) 400°C, (b) 700°C, (c) 900°C, (d) 1,000°C and e) 1,100°C for 5 h at 50000x magnification.

the catalytic activity of the catalyst will be higher and more active at reaction temperatures above 200°C.

3.1.6. Field Emission Scanning Electron Microscopy (FESEM) analysis

FESEM analysis was used to study the morphology of the RMS (5:35:60) catalyst supported on alumina. Fig. 6 displays the FESEM micrographs at 50000X magnification of the RMS (5:35:60) catalyst calcined at 400, 700, 900, 1,000 and 1,100°C for 5 h. The micrograph for different calcination temperatures showed no significant changes of morphology. As can be observed, the particles became more agglomerated with increasing calcination temperatures. The micrograph also showed that when the calcination temperature was raised to 1,000°C, the catalyst had more pores and this structure could help in the CO_2 methanation activity. From the morphology of the catalyst, it revealed more agglomeration occurred by providing higher surface areas for the active species to absorb the gasses which contributed to higher catalytic activity. At a calcination temperature of 400°C, the catalyst surface was tightly packed, which results in a small surface area, which limits the active sites of the methanation reaction and thus reduces the catalytic activity performance. At a calcination temperature of 1,000°C, micrographs showed that small spherical particles were agglomerated on the catalyst surface which can provide the highest catalytic activity.

3.1.7. Energy Dispersive X-ray (EDX) analysis

The composition of the element that was present on the catalyst surface was confirmed by EDX analysis. The EDX analysis revealed a low atomic ratio of Sm, Mn, and Ru with below than 1.00%. This is most likely due to the absorption of alkaline metal, Sm, Ru and Mn in highly porous and high surface area alumina beads. This is in agreement with the FESEM analysis which showed many pores on the surface. However, when the calcination temperature was raised to 1,000°C, the atomic ratio of each element increased which are Sm (0.72%), Mn (0.79%), except for Ru (0.37%). This is supported by the XRD where the peak of the RuO_2 species was very small in intensity. Previous research conducted by Zielinska et al., reported that the content of elements increased with the increasing calcination temperature [38]. However, when the catalyst was calcined at 1100°C, the element composition of Sm and Mn were slightly decreased with 0.49% and 0.64%, respectively except for the Ru element which showed an increase with 0.54%. This observation was corroborated by XRD analysis and again showed the appearance of the Mn and Ru in the catalyst samples.

3.1.8. Nitrogen Adsorption (NA) analysis

The pore structure and surface area analyses were measured by nitrogen adsorption analysis with the Brunauer–Emmett–Teller (BET) method. It was found that the BET surface area of the RMS (5:35:60) catalysts decreased with each increment of calcination temperature. The reduction of surface area among the catalysts might be due to agglomeration of metal oxide particles as shown by the FESEM analysis. At a 400°C calcination temperature, the BET surface area was higher by 155.03 m^2/g with a 89.66 nm average pore diameter, indicating a smaller particle size. This was verified by a H_2-TPR analysis (Fig. 3) in which the H_2 consumption showed a reduction at lower reduction temperature due to an increase in the particle dispersion [39]. When the calcination temperature was increased until 1000°C, the BET surface area showed only 41.36 m^2/g with an average pore diameter of 207.20 nm. Increasing the calcination temperature increases the pore size. This is due to the fact that large pores can lead to sintering, resulting in a decrease in pore volume and the formation of dense solid. Although, higher calcination temperatures reduce BET surface area, but have the advantage of ensuring the presence of a stable structure on the catalyst.

3.2. Catalytic Activity

3.2.1. Effect of calcination temperature

The screening of monometallic and bimetallic catalysts has been discussed in our previous study [40]. The lower CO_2 conversion for monometallic and bimetallic oxides has steered to the trimetallic oxide catalyst. However, the higher reaction temperature was not compatible with the requirement of industry to achieve a low reaction temperature. Thus, the effect of calcination temperatures on the potential catalyst of RMS (5:35:60) with respect to the catalytic performance using FTIR analysis was investigated. At 400, 700, 800 and 900°C, the CO_2 conversion were 94, 96, 89 and 91%, respectively. Meanwhile, at 1000°C calcination temperature, the CO_2 conversion showed a 100% CO_2 conversion, followed by 1,100°C, with a 98% which was slightly decreased at a maximum 400°C of reaction temperature. From the diffractograms in Fig. 1, the noticeable peaks of MnO_2, RuO_2 and Sm_2O_3 showed that these species contributed in determining higher catalytic activity (100%) of RMS (5:35:60) calcined at 1,000°C.

3.2.2. Effect of metal oxide based loadings

The next parameter step was to optimise the RMS (5:35:60) catalyst for various samarium loadings to observe its effect on the performance of catalyst. The ratios of 50–85 wt% of samarium oxide catalysts were selected. Low performance (< 30%) was observed for all the prepared catalysts (50–85 wt%) at 200°C reaction temperature except for the 60 wt% based loading which able to convert 65% of CO_2 at the same reaction temperature. It was clearly showed that an appropriate amount of samarium could increase the activity of the catalyst. As RMS (5:35:60) catalyst gives highest CO_2 conversion at 200 and 400°C reaction temperature (100%), it can be concluded that 60 wt% is the optimum loading for the samarium content. When the Sm content was increased beyond the optimum loading (60 wt%), the CO_2 conversion decreased. The excessive loading of Sm may block the active species on the catalyst surface as reported by He et al. [41]. Therefore, the trend for based loading is as follows: 50 < 55 < 85 < 80 < 75 < 70 < 65 < 60 wt%.

3.2.3. Effect of catalyst dosage

The parameters for various catalyst dosages were also investigated to find an optimum value for CO_2 conversion. The CO_2 conversion began to increase drastically at a reaction temperature of 200°C for each dosage. At a reaction temperature of 400°C with 3 g of catalyst or more, a complete CO_2 conversion (100%) was observed. Almost complete conversion of 98.53% occurred for 5 g of catalysts. This observation is mainly due to the increase in the number of active sites on the catalyst surface which are affected by the increase in the catalyst dosage. This finding was consistent with Su et al. [42], who found that when the catalyst dosage is increased, it would also increase the catalytic activity. Therefore, the catalyst dosage trend for CO_2 conversion was 3 < 5 < 7 g.

3.3. Methane Detection by Gas Chromatography

The potential catalysts selected from the screening process were further studied for the production of methane by GC analysis. No methane was produced at the initial temperature of 100°C for RMS (5:35:60) catalyst calcined at 1,000°C. However, when the reaction temperature was raised to 300, 350, and 400°C, about 31.11, 48.91 and 68.87% of methane production was detected. This indicates that the CH_4 content increases with increasing reaction temperatures. This might due to exothermic reactions which are required to form CH_4 at high reaction temperatures. Other than CH_4, the by-product of CH_3OH and H_2O were also formed from the reaction. Due to the high methane formation of RMS (5:35:60) calcined at 1,000°C, compared to the others, it was assigned as a potential catalyst among other studied samarium catalysts.

3.4. Reusability Test

Reusability test for the catalytic activity of RMS (5:35:60) catalyst was conducted by using the same catalyst several times until it deactivated through decreasing in catalytic activity of CO_2 conversion. The trend of reusability test for RMS (5:35:60) catalyst showed that after 5 times of reused catalyst, the CO_2 conversion started to decrease around 60%. All tested catalysts from 2 to 5 times showed a similar pattern with substantially increasing CO_2 conversion at 250°C till the highest examined reaction temperature, as shown in the Fig. S1. According to a study conducted by Argyle and Bartholomew, carbon deposition could occur when the catalyst was run repeatedly numerous times [43]. This is because carbon can chemisorb aggressively as a monolayer or physically adsorb in a multilayer, thus blocking the reactant from reaching metal surface sites.

3.5. Statistical Analysis of $Ru/Mn/Sm/Al_2O_3$

3.5.1. Artificial neural network

In this study, a neural network technique was applied to develop the best CO_2 conversion prediction model using three hidden nodes. The ANN model was trained using the Levenberg Marquardt Learning Algorithm. The factors were calcination temperature, °C (900–1,100°C), based ratio, % (60–80%), and catalyst dosage, g (3–7 g). The parameters were selected based on preliminary results. Table 1 shows the experimental and predicted values for CO_2 conversion.

In general, the percentages of CO_2 conversion obtained were high. The efficiency test of modelling was also was performed to validate the quality of the model between predicted and measured values. Based on the findings, almost all prediction values for CO_2 conversion were near to 1. According to Nash and Sutcliffe [19] and Grunwald and Frede [44], the closer the model efficiency is to 1, the more accurate the model. Table 2 summarizes the statistical parameters of the selected ANNs: Number of hidden nodes, R^2, RMSE and sum frequency. Selection of the network for prediction of CO_2 conversion was carried out with a trial-and-error technique. The optimal number of hidden nodes is three. The training and validation of R^2 and RMSE values are 0.99/0.32 and 0.99/0.22, respectively.

Then, the equation for CO_2 conversion calculation was developed based on the ANN analysis. The equation can be expressed as in Eq. (4)–(6):

Firstly, the calculation of three hidden nodes was performed:

$$H1 = \tanh(.5 * (-0.0449 * Calcination\_Temperature + -0.0014 * Based\_Ratio + -0.0752 * Catalyst\_Dosage + 49.9550)); \quad (4)$$

Table 1. Experiment Design for CO_2 Conversion and ANN Results for Samarium Catalyst

Calcination Temperature X_1 **(°C)**	Based Ratio X_2 **(%)**	**Catalyst Dosage** X_3 **(g)**	**CO_2 Conversion (%) - Actual**	**CO_2 Conversion (%) - ANN**	**Effeciency Test of modelling**
1,000	70	5	98.77	98.82	0.99
1,100	70	3	91.01	91.38	0.95
1,000	60	7	100.00	100.10	1.08
1,100	70	7	92.75	93.17	0.93
1,100	80	5	89.70	89.62	1.01
900	70	3	89.87	90.10	0.97
900	60	5	91.20	90.91	1.04
1,000	80	3	96.80	96.89	0.95
1,000	60	5	98.53	98.48	1.21
1,100	60	5	95.23	94.93	1.08
1,000	60	3	100.00	100.20	1.16
1,000	80	7	98.18	98.00	1.30
1,100	70	5	99.35	99.45	1.17
1,000	70	3	98.99	98.96	0.84
1,000	80	5	98.27	98.32	0.90
900	70	7	90.28	90.48	0.98
900	80	5	89.80	89.74	1.01

$$H2 = \tanh(.5 * (-0.0381 * Calcination\_Temperature + -0.3907 * Based\_Ratio + 1.9902 * Catalyst\_Dosage + 55.2766)); \quad (5)$$

$$H3 = \tanh(.5 * (0.0155 * Calcination\_Temperature + -0.1863 * Based\_Ratio + 0.8939 * Catalyst\_Dosage + -7.1390)); \quad (6)$$

Lastly, the prediction model of CO_2 conversion was calculated using Eq. (7):

$$CO2\ Conversion\ (Prediction) = 82.6831 + (16.5478 * H1) + (-9.0167 * H2) + (11.5466 * H3) \quad (7)$$

where, H1, H2 and H3 represent the hidden nodes.

Table 2. The summary of ANN Analysis

Training		**Validation**	
R^2	0.99	R^2	0.99
RMSE	0.32	RMSE	0.22
Number of Hidden Nodes	3	Number of Hidden Nodes	3
SSE	1.45	SSE	0.14
Sum Freq	14	Sum Freq	3

4. Conclusions

The catalyst of RMS (5:35:60) calcined at 1,000°C gave 100% CO_2 conversion with 68.87% of CH_4 formation at a 400°C reaction temperature. The high CO_2 conversion obtained was due to existence of active species on the catalyst surface. Other than that, the predicted value obtained from the ANN is almost identical with the experimental data by R^2 values of CO_2 conversion at 0.99. This showed that the models provide a reliable outcome and the equation generated from the ANN can be used to predict the CO_2 conversion for other value in range of studied parameter. The optimum conditions from the ANN also revealed the RMSE value for training and validation are 0.32 and 0.22, respectively which indication of accuracy of model.

Acknowledgment

The authors thank to Universiti Sultan Zainal Abidin, and Universiti Teknologi Malaysia for GUP grant vote 13H34.

Conflict-of-Interest

The authors declare no conflict of interest.

Author Contributions

S.J.M.R. (Ph.D) conducted the experiment in catalytic activity, A.A. (Ph.D) doing statistical analysis using ANN, S.T. (Ph.D) doing the characterisation catalyst, W.A.W.A.B. (Ph.D) doing the proofread and content arrangement, A.Z.A.H. (Ph.D) doing the characterisation catalyst, W.N.A.W.M. (Ph.D) doing the characterisation catalyst, A.F.A. (MSc. Student) doing analysis and statistical analysis using ANN, N.Z. (MSc. student) doing analysis and statistical analysis using ANN and S.M.R. (MSc. student) formatted and revise the manuscript.

Nomenclature

CO_2	carbon dioxide

CH_4	methane
H_2	hydrogen
CO	Carbon monoxide
XRD	X-ray diffraction
Sm_2O_3	samarium (III) oxide
MnO_2	manganese (IV) oxide
Sm	samarium
Mn	manganese
Ru	ruthenium
Al	aluminium
RMS	$Ru/Mn/Sm/Al_2O_3$
$MnNO_3$	Manganese (III) nitrate
$RuCl_3$	Ruthenium (III) chloride
Al_2O_3	Aluminium oxide
CH_3OH	methanol
TPR	Temperature Programme Reduction
TPD	Temperature Programme Desorption
FESEM	Field Emission Scanning Electron Microscopy
EDX	Energy Dispersive X-ray
XPS	X-ray photoelectron spectroscopy
GC	Gas chromoatography
ESR	Electron Spin Resonance
FTIR	Fourier Transform Infrared
ANN	artificial neural network
MLP-ANN	Multi-layer perception artificial Neural Netwok

References

1. Rosid SJM, Toemen S, Asif Iqbal MM, Bakar WAWA, Mokhtar WNAW, Aziz MMA. Overview performance of lanthanide oxide catalysts in methanation reaction for natural gas production. *Environ. Sci. Pollut. Res.* 2019;26:36124–36140. https://doi.org/10.1007/s11356-019-06607-8.
2. Wang SG, Liao XY, Cao DB, et al. Factors controlling the interaction of CO_2 with transition metal surfaces. *J. Phys. Chem. C.* 2007;111:16934-16940. https://doi.org/10.1021/jp074570y.
3. Yamasaki M, Komori M, Akiyama E, et al. CO_2 methanation catalysts prepared from amorphous Ni-Zr-Sm and Ni-Zr-misch metal alloy precursors. *Mater. Sci. Eng. A.* 1999;267:2:220-226. https://doi.org/10.1016/S0921-5093(99)00095-7.
4. Le Dimet FX, Souopgui I, Ngodock HE. Sensitivity analysis applied to a variational data assimilation of a simulated pollution transport problem. *Int. J. Numer. Methods Fluids*. 2017;83:5:465-482. https://doi.org/10.1002/fld.4274.
5. Yusof KMKK, Azid A, Jamalani MA. Determination of significant variables to particulate matter (pm10) variations in northern region, Malaysia during haze episodes (2006-2015). *J. Fundam Appl. Sci*. 2018;10:1S:300-312.
6. Azid A, Juahir H, Toriman ME, et al. Prediction of the level of air pollution using Principal Component Analysis and Artificial Neural Network Techniques: a case study in Malaysia. *Water Air Soil Pollut*. 2014;225:8:2063. https://doi.org/10.1007/s11270-014-2063-1.
7. Zamaniyan A, Joda F, Behroozsarand A, Ebrahimi H. Application of artificial neural networks (ANN) for modelling of industrial hydrogen plant. *Int. J. Hydrog. Energy*. 2013;38:6289-6297. https://doi.org/10.1016/j.ijhydene.2013.02.136.
8. Alsaffar MA, Mageed AK, Abdel Ghany MAR, Ayodele BV, Mustapa SI. Elucidating the non-linear effect of process parameters on hydrogen production by catalytic methane reforming: an artificial intelligence approach. *IOP Conf. Ser.: Mater. Sci. Eng*. 2020;99:1012078. https://doi.org/10.1088/1757-899X/991/1/012078
9. Ngo SI, Lim Y-I. Solution and Parameter Identification of a Fixed-Bed Reactor Model for Catalytic CO_2 Methanation Using Physics-Informed Neural Networks. *Catalysts* 2021;11:1304. https://doi.org/10.3390/catal11111304
10. Esfandyari M, Amiri M, Koolivand-Salooki M. Neural Network prediction of the Fischer-Tropsch synthesis of natural gas with Co (lll)/Al_2O_3 catalyst. *Chem. Eng. Res. Bull.* 2015;17:25-33. https://doi.org/10.3329/cerb.v17i1.22915.
11. Toemen S, Sulaiman SF, Rosid SJM, et al. Effectiveness of Ru/Mg/Ce Supported on Alumina Catalyst for Direct Conversion of Syngas to Methane: Tailoring Activity and Physicochemical Studies. *Arab. J. Sci. Eng*. 2021. https://doi.org/10.1007/s13369-021-06300-4
12. Asif Iqbal MM, Toemen S, Bakar WAWA, Razak FIA, Rosid SJM, Azelee NIW. Catalytic methanation over nanoparticle heterostructure of Ru/Fe/Ce/g-Al_2O_3 catalyst: Performance and characterization. *Renew. Energy*. 2020;162:513-524. https://doi.org/10.1016/j.renene.2020.06.093.
13. Azid A, Juahir H, Latif MT, Zain SM, Osman MR. Feed-Forward Artificial Neural Network Model for Air Pollutant Index Prediction in the Southern Region of Peninsular Malaysia. *J. Environ. Prot. Sci*. 2013;4:1-10. https://doi.org/10.4236/jep.2013.412A1001.
14. Azaman F, Azid A, Juahir H, et al. Application of artificial neural network and response surface methodology for modelling of hydrogen production using nickel loaded zeolite. *J. Teknol*. 2015;77:1:109-118. https://doi.org/10.11113/jt.v77.4265.
15. Isiyaka HA, Juahir H, Toriman ME, et al. Spatial assessment of air pollution index using environ metric modeling techniques. *Adv. Environ. Biol*. 2014;8:24:244-256. https://doi.org/10.11113/jt.v75.3977
16. Azid A, Juahir H, Toriman ME, et al. Selection of the most significant variables of air pollutants using sensitivity analysis. *J Test Eval*. 2016;44:1:376-384. https://doi.org/10.1520/JTE20140325.
17. Rosid SJM, Bakar WAWA, Ali R. Characterization and modelling optimization on methanation activity using Box-Behnken design through cerium doped catalysts. *J. Clean. Prod*. 2018;170:278-287. https://doi.org/10.1016/j.jclepro.2017.09.073
18. Azid A, Rani NLA, Samsudin MS, et al. Air quality modelling using chemometric techniques. *J. Fundam. Appl. Sci*. 2017;9:2S:443-466. https://doi.org/10.4314/jfas.v9i2s.30
19. Nash JE, Sutcliffe JV. River flow forecasting through conceptual models, Part I - A discussion of principles, *J. Hydrol*. 1970;10:282–290. https://doi.org/10.1016/0022-1694(70)90255-6.
20. Rosid SJM, Bakar WAWA, Ali R. Physicochemical study of supported cobalt–lanthanum oxide-based catalysts for CO_2/H_2 methanation reaction. *Clean Techn Environ Policy*. 2015;17:257–264. https://doi.org/10.1007/s10098-014-0766-z.
21. Xu B, Wei J, Yu Y, Li J, Zhu Q. Size Limit of Support Particles

in an Oxide-Supported Metal Catalyst: Nanoparticles Ni/ZrO_2 for Utilization of Natural Gas. *J. Phys. Chem, B*. 2003;107: 5203-5207. https://doi.org/10.1021/JP030127L.
22. Nguyen TD, Mrabet O, Do TO. Controlled self-assembly of Sm_2O_3 nanoparticles into nanorods: Simple and large-scale synthesis using bulk Sm_2O_3 powders. *J. Phys. Chem C*. 2008;112: 15226-15235. https://doi.org/10.1021/jp804030m.
23. Toemen S, Bakar WAWA, Ali R. Effect of ceria and strontia over Ru/Mn/Al_2O_3 catalyst: Catalytic methanation, physicochemical and mechanistic studies. *J. CO_2 Util*. 2016;13:38-49. https://doi.org/10.1016/j.jcou.2015.11.005.
24. Chung J, Park JH, Park JG, et al. Photoemission study of rare earth ditelluride compounds ($ReTe_2$: Re = La, Pr, Sm, and Gd). *J Korean Phys Soc*. 2001;38:6:744-749. https://arxiv.org/abs/cond-mat/9910443v1.
25. Suzuki C, Kawai J, Takahashi M, Vlaicu AM, Adachi H, Mukoyama T. The electronic structure of rare earth oxides in the creation of the core hole. *Chem. Phys*. 2000;253:27-40. https://doi.org/10.1016/S0301-0104(99)00380-8.
26. Nguyen TD, Dinh CT, Do TO. Monodisperse samarium and cerium orthovanadate nanocrystals and metal oxidation states on the nanocrystals surface. *Langmuir*. 2009;25:18:11142-11148. https://doi.org/10.1021/la901387q.
27. Bao X, Jiang Z, Zhou W, Tan D, Zhai R. Evidence for perimeter sites over SmOx-modified Rh(100) surface by CO chemisorption. *Surf. Sci*. 2004;565:269-278. https://doi.org/10.1016/j.susc.2004.07.021.
28. Chakradhar PS, Murali A, Rao JL. A study of electron paramagnetic resonance and optical absorption in calcium manganese phosphate glasses containing praseodymium. *J. Mater. Sci*. 2000;35:353-359. https://doi.org/10.1023/A:1004713805467.
29. Phan TL, Zhang P, Tran HD, Yu SC. Electron spin resonance study of Mn-doped metal oxides annealed at different temperatures. *J. Korean Phys. Soc*. 2010;57:5:1270-1276. https://doi.org/10.3938/jkps.57.1270.
30. Liu J, Liu J, Zhao Z, Wei Y, Song W. Fe-Beta@CeO_2 Core-Shell Catalyst with Tunable Shell Thickness for Selective Catalytic Reduction of NO_x with NH_3. *AIChE J*. 2017;63(10):4430-4441. https://doi.org/10.1002/aic.15743..
31. Li YW, He D, Zhu Z, Zhu Q, Xu B. Properties of Sm_2O_3-ZrO_2 composite oxides and their catalytic performance in isosynthesis. *Appl. Catal. A-Gen*. 2007;319:119-127. https://doi.org/10.1016/j.apcata.2006.11.020.
32. Peluso MA, Hernandez WY, Dominguez MI, Thomas HJ, Centeno MA, Sambeth JE. CO oxidation: Effect of Ce and Au addition on MnOx catalysts. *Lat. Am. Appl. Res*. 2012;42: 351-358. http://hdl.handle.net/10261/98974.
33. Gandia LM, Vicenta MA, Gil A. Preparation and characterization of manganese oxide catalysts supported on alumina and zirconia-pillared clays. *Appl Catal A-Gen*. 2000;196:281-292. https://doi.org/10.1016/S0926-860X(99)00479-2.
34. Djebaili K, Mekhalif Z, Boumaza A, Djelloul. XPS, FTIR, EDX, and XRD analysis of Al_2O_3 scales grown on PM2000 alloy. *J. Spectrosc*. 2015;1-16. https://doi.org/10.1155/2015/868109.
35. Lin WW, Cheng HY, Ming J, Yu YC, Zhao FY. Deactivation of Ni/TiO_2 catalyst in the hydrogenation of nitrobenzene in water and improvement in its stability by coating a layer of hydrophobic carbon. *J. Catal*. 2012;291:149-154. https://doi.org/10.1016/j.jcat.2012.04.020.
36. Meng F, Zhong P, Li Z, Lui X, Zheng H. Surface structure and catalytic performance of Ni-Fe catalyst for Low-tempertature CO hydrogenation. *J. Chem*. 2014;1-7. https://doi.org/10.1155/2014/534842.
37. Cox PA. The element on Earth-Inorganic Chemistry in the Environment. Oxford. Oxford University Press. 1995. p. 147-158.
38. Zielinska B, Mijowska E, Kalenczuk RJ. Synthesis and characterization of K-Ta mixed oxides for hydrogen generation in photocatalysis. *Int. J. Photoenergy*. 2012;1-7. https://doi.org/10.1155/2012/525727.
39. Pojanavaraphan C, Luengnaruemitchai A, Gulari E. Catalytic activity of Au-Cu/CeO_2-ZrO_2 catalysts in steam reforming of methanol. *Appl. Catal. A-Gen*. 2013;456:135-143. https://doi.org/10.1016/j.apcata.2013.02.010.
40. Rosid SJM, Abu Bakar WAW, Ali R. Methanation Reaction over Samarium Oxide Based Catalysts. *Mal. J. Fund. Appl. Sci*. 2013;9:1:28-34. https://doi.org/10.11113/mjfas.v9n1.78.
41. He HQ, Zhang L, Wu H, Li CZ, Jig SP. Synthesis and characterization of doped La9ASi6026.5 (A= Ca,Sr,Ba) oxy apatite electrolyte by water-based gel-casting route. *Int. J. Hydrog. Energy*. 2011;36:11:6862-6874.
42. Su P, Chu O, Wang L. Studies on catalytic activity of nanostructure Mn_2O_3 prepared by solvent-thermal method on degrading crystal violet. *Mod. Appl. Sci*. 2010;4:5:125-129. https://doi.org/10.5539/mas.v4n5p125.
43. Argyle MD, Bartholomew CH. Heterogeneous catalyst deactivation and regeneration: A review. *Catalysts* 2015;5:145-269. https://doi.org/10.3390/catal5010145.
44. Grunwald S, Frede H-G. Using the modified agricultural non-point source pollution model in German Watershed. *Catena* 1999;37:319-328. https://doi.org/10.1016/S0341-8162(99)00024-7.